Image Analysis and Processing with Applications in Proteomics and Medicine

Eleftheria A. Mylona*

National and Kapodistrian University of Athens
Department of Informatics and Telecommunications
emylona@di.uoa.gr

Abstract. This thesis introduces unsupervised image analysis algorithms for the segmentation of several types of images, with an emphasis on proteomics and medical images. The presented algorithms are tailored upon the principles of deformable models, with an emphasis on region-based active contours. Two different objectives are pursued. The first is the core issue of unsupervised parameterization in image segmentation, whereas the second is the formulation of a complete model for the segmentation of proteomics images, which is the first to exploit the appealing attributes of active contours. The first major contribution is a novel framework for the automated parameterization of region-based active contours. The presented framework aims to endow segmentation results with objectivity and robustness as well as to set domain users free from the cumbersome and time-consuming process of empirical adjustment. It is applicable on various medical imaging modalities and remains insensitive on alterations in the settings of the acquisition devices. The experimental results demonstrate that the presented framework maintains a segmentation quality which is comparable to the one obtained with empirical parameterization. The second major contribution is an unsupervised active contour-based model for the segmentation of proteomics images. The presented model copes with crucial issues in *2D-GE* image analysis including streaks, artifacts, faint and overlapping spots. In addition, it provides an alternate to the laborious, error-prone process of manual editing, which is required in state-of-the-art *2D-GE* image analysis software packages. The experimental results demonstrate that the presented model outperforms *2D-GE* image analysis software packages in terms of detection and segmentation quantity metrics.

Keywords: Segmentation, Active Contours, Proteomics Images, Medical Images.

1   Introduction

Segmentation is a challenging task in image analysis with essential applications in biomedical engineering, remote sensing, robotics and automation. Typically, the

*Dissertation Advisor: Dimitris Maroulis, Professor

target region is separated from the rest of image regions utilizing defining features including intensity, texture, color or motion cues. Moreover, the separation of the target regions is impeded by several daunting factors such as: background clutter, the presence of noise and artifacts as well as occlusions on multiple target regions. This thesis focuses on image segmentation using deformable models and specifically region-based Active Contours (*ACs*) [1] because of their strong mathematical foundation and their appealing properties.

ACs are formulated according to an energy functional defined so as to be minimized when approximating target boundaries. The argument of the energy functional is typically a curve or surface, which evolves and defines the partitioning of the image based on external forces that hinge on image features such as intensity and/or texture. Additionally, internal constraints generate tension and stiffness, which preserve the smoothness and continuity of the model by preventing the formation of sharp corners. The corresponding Euler-Lagrange equation constitutes a Partial Differential Equation (*PDE*), i.e. an iterative gradient descent algorithm, which guides the evolution towards the minimum. The numerical implementation of the evolution is performed by the level set method, which endows the model with topological adaptability, i.e. splitting or merging, appearing or disappearing during the surface evolution.

In this thesis, a novel framework for automated region-based *AC* parameterization is developed, aiming to endow segmentation results with objectivity and robustness as well as to set domain users free from the cumbersome and time-consuming process of empirical parameter adjustment. In addition, an unsupervised *AC*-based model for the segmentation of proteomics images is developed to provide an alternate to the laborious, error-prone process of manual editing by gel analysts.

All ideas presented in this thesis have been published [2],[3], accepted with revisions [4] and submitted [5] in four (4) international peer-reviewed journals, eleven (11) international peer-reviewed conferences [6]-[16], one (1) book chapter [17] and one (1) Hellenic conference [18].

2 Proposed Framework for Automated Parameterization of Region-Based *ACs*

ACs are a rather mature image segmentation paradigm, with several variations proposed in literature. However, their parameterization remains a challenging, open issue, with strong implications on the quality, objectivity and robustness of the segmentation results. Very often, parameters are empirically adjusted on a trial and error basis, a process which is laborious and time-consuming, based on subjective as well as heuristic considerations. On one hand, non-expert users such as Medical Doctors (*MDs*) and biologists require technical support since they are not familiar with the algorithmic inner mechanisms. On the other hand, parameter configurations empirically determined by image analysis experts are usually suboptimal and applicable to specific datasets. A novel framework is proposed for automated adjustment of region-based *AC* regularization and data fidelity parameters based on local image geometry information. Starting from the observation that these parameters

and the eigenvalues of structure tensors are associated with the same orthogonal directions, local image geometry is encoded by the orientation coherence in edge regions. The latter can be mined by means of Orientation Entropy (*OE*), a measure which is an increasing function of the variability in edge orientation, obtaining low values in structured regions containing edges of similar orientations and high values in unstructured regions containing edges of multiple orientations. *OE* is calculated on directional subbands in each scale of the Contourlet Transform (*CTr*) [19], which apart from intensity also represents textural information. As a result, those forces that guide contour away from randomly oriented, high-entropy edge regions are amplified and iterations dedicated to misleading local minima are avoided, speeding up contour convergence. On the other hand, forces imposed within the proximity of structured edges, naturally related to target edge regions, are reduced, enhancing segmentation accuracy.

In the context of the proposed framework, each $q \times q$ image block is fed into the *CTr* filter-bank through an iterative procedure and is decomposed into one pyramidal level, which is then transformed into four directional subbands: 0°, 45°, 90° and 135°. The band-pass directional subbands represent the local image structure. *OE* is calculated on each directional subband image I_{jk} as follows:

$$OE_{jk} = -\sum_{n=1}^{N_{jk}} \sum_{m=1}^{M_{jk}} p_{jk}(m,n) \cdot \log p_{jk}(m,n) \tag{1}$$

$$p_{jk}(m,n) = \frac{|I_{jk}(m,n)|^2}{\sqrt{\sum_{n=1}^{N_{jk}} \sum_{m=1}^{M_{jk}} [I_{jk}(m,n)]^2}} \tag{2}$$

where OE_{jk} is the *OE* of the subband image I_{jk} in the kth direction and the jth level of decomposition, M_{jk} is the row size and N_{jk} the column size of the subband image. Among the *OE* values calculated for each subband image, the maximum value OE_{jk} of the most informative direction k is calculated and assigned to all pixels of the corresponding block. The result is considered as an *OE* 'heatmap' reflecting local image structure.

Regularization and data fidelity parameters are matrices of the same dimensions as the original image, and are calculated according to the following equations:

$$w_{reg}^{auto} = a \cdot (\frac{1}{w_{df}^{auto}}), \quad w_{df}^{auto} = \arg_{I_{jk}} \max(OE_{jk}(I_{jk})) \tag{3}$$

where *a* depends on the dimensions of the image block. The core idea is to guide the active contour towards structured, target edge regions in the early stages of evolution by appropriately amplifying data fidelity forces in randomly oriented, high-entropy regions. As a result the contour will be repelled and iterations dedicated to misleading local minima will be bypassed, speeding up contour convergence towards target

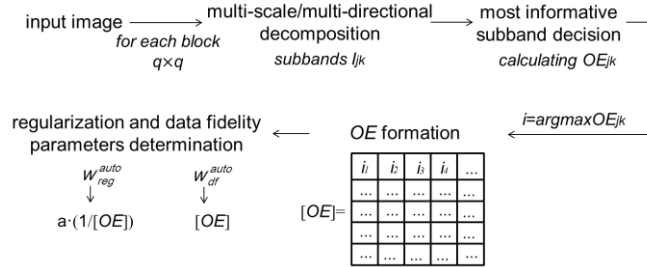edges. The pipeline of the presented framework is portrayed in the block diagram of Fig. 1.

Fig. 1. Block diagram of the pipeline of the presented framework.

The presented framework has been integrated into two region-based [1], [20] and one hybrid [21] *AC* model, in order to evaluate the segmentation performance of the automated versus empirical parameterization. Experiments are conducted on databases of natural and textured images as well as on various medical imaging modalities (mammograms, thyroid ultrasound images, endoscopy images, dermoscopy images, *CT*-scans of lung parenchyma, labial teeth and gingiva photographic images) so as to confirm the framework's generality with respect to image content. The shape of all abnormalities on medical images as well as the irregularity of their margins are malignancy risk factors which are highly considered by *MDs* before proceeding to fine needle aspiration biopsy. Fig. 2 illustrates segmentation results obtained by the automated version on samples of the utilized databases, as well as by the empirically fine-tuned version. The segmentation results depicted in Fig. 2 demonstrate that the presented framework achieves *comparable segmentation quality* to the one obtained by the empirically fine-tuned version *in an automated fashion*. The experimental results are quantitatively evaluated by means of two metrics: the Tanimoto Coefficient (*TC)* [22] and the Hausdorff distance *H* [23] defined as:

$$TC = \frac{N(A \cap B)}{N(A \cup B)}, \quad H(A,B) = \max_{a \in A} \min_{b \in B} \| a - b \| \tag{4}$$

where *A* is the ground truth set, *B* the set under evaluation, *N()* indicates the number of pixels of the enclosed region and *a, b* the points defined in sets *A, B*, respectively. Table 1 presents *TC* and *H* values, obtained by both versions, for each utilized database. The automated version achieves an average *TC* and *H* value of 83.1±1.4% and 40.9±1.8 mm, respectively *with regards to all images tested*, which is comparable to the *TC* and *H* value of 82.0±1.5% and 42.3±3.8 mm respectively obtained by the empirically fine-tuned version. This comparable segmentation accuracy verifies the value of the presented framework for automated parameter adjustment, without the need for laborious fine-tuning from *MDs*.
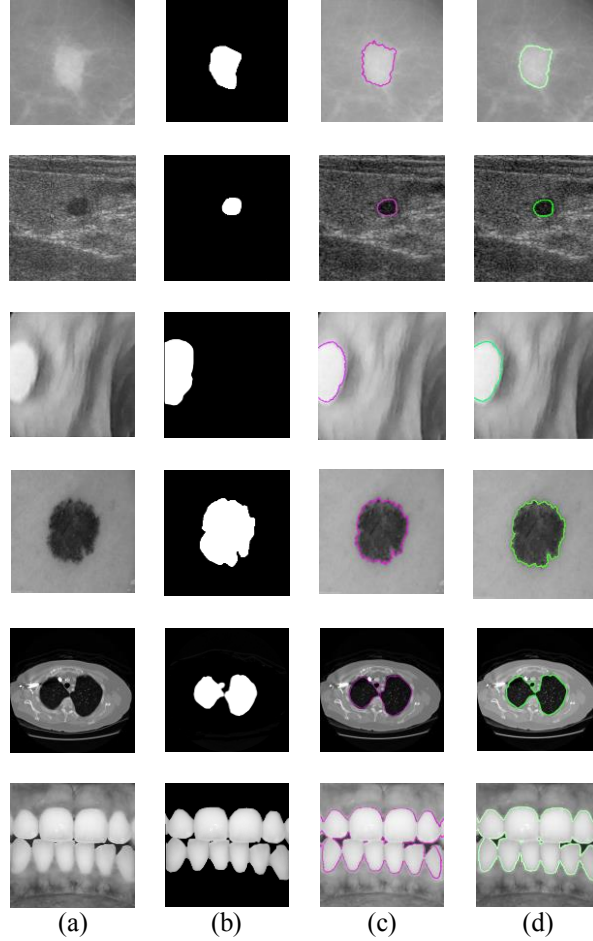
Fig. 2. (a) Sample images of the utilized databases, (b) corresponding ground truth images, (c) segmentation results of the empirically fine-tuned version, (d) segmentation results of the automated version.

Table 1: *TC* and *H* values for each utilized database

Database	TC (%)		H (mm)	
	Empirical	**Automated**	**Empirical**	**Automated**
Mini-MIAS	82.3±1.8	83.4±1.2	42.3±2.5	41.2±1.7
Thyroid US	82.8±1.2	83.7±0.8	43.7±3.3	41.7±2.1
Endoscopy	81.4±1.5	82.3±1.4	41.4±3.8	40.8±1.3
Dermoscopy Atlas	81.7±0.9	82.8±1.6	41.2±4.2	40.1±1.5
CT scans	80.2±1.5	81.8±1.7	40.7±2.6	39.3±2.2
LTG-IDB	82.9±1.6	84.2±1.8	44.8±5.7	42.4±2.5

3   Unsupervised *AC*-Based Model for the Detection and Segmentation of Proteomics Images

In this thesis, a novel analysis method is also presented for the detection and segmentation of protein spots in *2D-GE* images. This is the first complete analysis model exploiting the appealing properties of the *AC* formulation in order to cope with crucial issues in *2D-GE* image analysis, including the presence of noise, streaks, multiplets and faint spots. In addition, it is unsupervised, providing an alternative to the laborious, error-prone process of manual editing, which is still required in state-of-the-art *2D-GE* image analysis software packages.

The detection technique utilizes the dilation image operator, which embeds a disk-shaped Structuring Element (*SE*) [24], adjusted to the dominant roundish shape of protein spots. The disk-shaped *SE* limits the falsely detected streaks. *SE* size is set considering that a certain radius value minimizes the detection of false negatives, whereas it allows the detection of local maxima associated with small spots, even in cases where they overlap with larger spots in complex regions.

The accompanying segmentation scheme comprises four main processes, namely: (a) a detection process capable of identifying boundaries of spot overlap in regions occupied by multiplets, based on the observation that such boundaries are associated with local intensity minima, (b) histogram adaptation and morphological reconstruction so as to avoid unwanted amplifications of noise and streaks, as well as to facilitate the identification of faint spots, (c) a contour initialization process aiming to form a level set surface initializing the subsequent level set evolution, based on the observation that protein spots are associated with regional intensity maxima and (d) a level set evolution process guided by region-based energy terms determined by image intensity as well as by information derived from the previous processes.

The presented technique has been experimentally evaluated on a dataset of 13 real *2D-GE* images, containing approximately 26.000 protein spots. This dataset of images was provided by the Biomedical Research Foundation of the Academy of Athens. Melanie 7 [25] software package is used for comparisons. Fig. 3 illustrates: (a) the ground truth image, (b) detection results obtained by Melanie 7 software package and (c) detection results obtained by the presented detection technique. It can be observed that, much more actual protein spots are missed (red arrows), whereas more artifacts are falsely detected as spots (green arrow) by Melanie 7 software package.
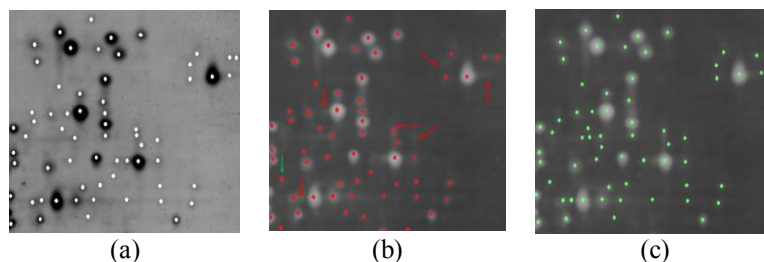

| (a) | (b) | (c) |

Fig. 3. (a) Ground truth image, (b) detection results obtained by Melanie 7, (c) detection results obtained by the presented detection technique.

The detection results are quantified by means of the Predictive Value (*PV*), Specificity (*SP*) and Detection Sensitivity (*DS*), which are defined as:

$$PV = \frac{TP}{TP + FP}, \quad SP = \frac{TN}{TN + FP}, \quad DS = \frac{TP}{FN + TP} \quad (5)$$

where *TP, TN, FN* are defined as true positive, true negative and false negative spots. Table 2 presents the *PV, SP* and *DS* obtained by the presented detection technique and Melanie 7, in a total of approximately 26.000 protein spots appearing in the dataset of 13 *2D-GE* images. Considering the experimental evaluation it can be concluded that the presented detection technique achieves a *PV,* a *SP* and a *DS* which exceed 80%, outperforms Melanie 7, distinguishes multiple overlapping spots, locates spots within streaks and ignores artifacts.

Table 2: Overall detection results obtained by Melanie 7 and the presented detection technique

	Melanie 7	**Presented Detection Technique**
PV(%)	73.6±17.4	88.2±4.2
SP(%)	33.2±13.5	81.6±5.3
DS(%)	77.4±12.6	87.3±6.2

In the context of protein spot segmentation, the presented segmentation scheme is based on the Chan-Vese model [1] and comprises four main processes: (a) separation of multiplets, (b) histogram adaptation and morphological reconstruction, (c) level set initialization and (d) contour evolution. The original *2D-GE* image is scanned with parallel straight-line segments of variable lengths and multiple directions, so as to facilitate the detection of local intensity minima, associated with each particular direction. Local intensity minima are identified for each parallel straight-line segment. Fig. 4 illustrates: a) a real *2D-GE* image, b) the detection results obtained by the local intensity minima process, with each minimum marked as black. It is evident that, the detection process actually identifies boundaries of spot overlap. Therefore, alterations in the pre-processing techniques as well as further manual editing are not required.
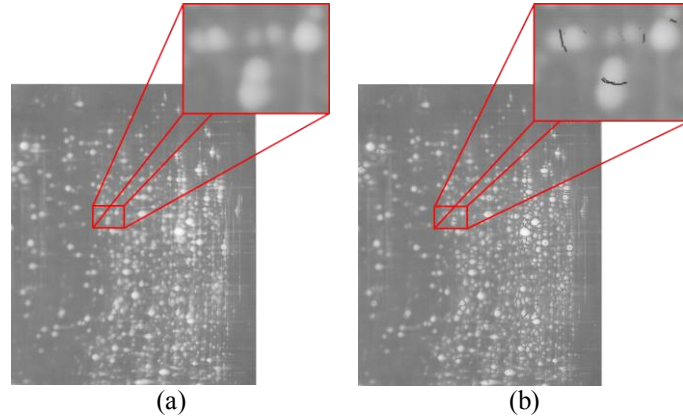
Fig. 4. (a) Real *2D-GE* image, (b) detection results obtained by the local intensity minima process.

A popular histogram equalization variant called Contrast-Limited Adaptive Histogram Equalization (*CLAHE*) [26] is utilized to enhance the segmentation performance of the presented scheme with respect to the presence of faint spots in *2D-GE* images. The enhanced image is binarized according to a threshold value and the flood-fill morphological operation is applied so as to eliminate holes as a result of intensity inhomogeneity. Fig. 5 illustrates the results obtained by the flood-fill morphological operation on: (a) the *2D-GE* image illustrated in Fig. 4(b), (b) the enhanced image which is generated by the application of *CLAHE*. It is evident that, the utilization of *CLAHE* is essential, since most faint spots are missed when *CLAHE* is omitted.
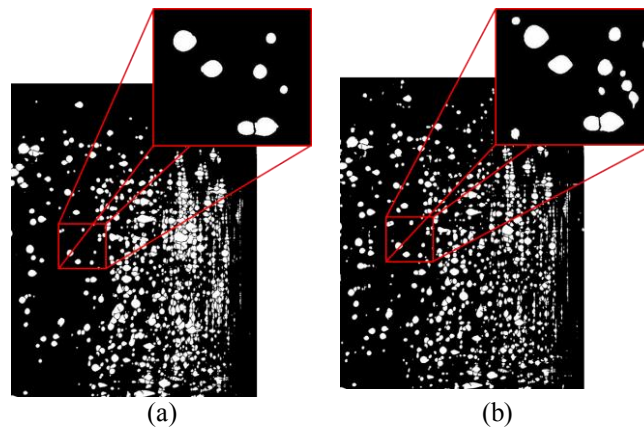

Fig. 5. Results obtained by the flood-fill morphological operation on: (a) the image illustrated in Fig. 4(b), (b) on the enhanced image which is generated by the application of *CLAHE*.

The level set function is initialized so that the associated zero levels approximate the actual protein spots. Starting from the observation that regional intensity maxima of a *2D-GE* image are associated with protein spots, the presented initialization process constructs a level set surface of multiple cones centered at maxima positions. This surface can serve as a spot-targeted initialization of the level set function. Aiming to enhance segmentation performance, contour evolution is initialized by the spot-targeted level set surface generated by the previous initialization process. The *AC* converges according to the following equation:

$$
\begin{aligned}
\frac{\partial \varphi}{\partial t} = {} & w_{reg}^{fixed} \cdot \delta(\varphi(x,y)) \cdot div\left(\frac{\nabla \varphi}{|\nabla \varphi|}\right) \\
& - w_{df_1}^{fixed} \cdot (I_1(x,y) - c_1)^2 + w_{df_1}^{fixed} \cdot (I_1(x,y) - c_2)^2 - \\
& - w_{df_2}^{fixed} \cdot (I_2(x,y) - c_3)^2 + w_{df_2}^{fixed} \cdot (I_2(x,y) - c_4)^2
\end{aligned}
\tag{6}
$$

where I_1, I_2 are the original image and the binarized image which is the output of morphological processing, respectively, c_1, c_2 and c_3, c_4 the average intensities inside and outside of the contour of I_1 and I_2, respectively.

The experimental evaluation of the presented segmentation scheme has been conducted on the dataset of 13 real digital grayscale *2D-GE* images provided by the Biomedical Research Foundation of the Academy of Athens, as well as on a dataset of 30 synthetic *2D-GE* images, so as to facilitate qualitative and quantitative comparisons with state-of-the-art *2D-GE* image analysis software packages. Fig. 6 illustrates segmentation results obtained by the application of Melanie 7 [25], Delta2D, PDQuest 8.0.1 [27] and the presented segmentation scheme on a real *2D-GE* image. It is evident that, the presented segmentation scheme results in more plausible spot boundaries than all three image analysis software packages. PDQuest 8.0.1 results in elliptical boundaries, which do not correspond to the irregular shape of the actual spot boundaries, whereas such elliptical boundaries tend to include background regions. In the cases of Melanie 7 and Delta2D, the obtained segmentation results suffer from over-segmentation and are subject to laborious, error-prone and time-consuming correction process by the expert biologists.

In order to quantitatively evaluate the presented segmentation scheme, experiments were performed on the set of synthetic images generated by the synthetic *2D-GE* image generation software, developed by the Real-time Systems & Image Analysis Lab of our Department. The segmentation performances are quantitatively evaluated in terms of Volumetric Overlap (*VO*) and Volumetric Error (*VE*), which are defined as follows:

$$
VO = \frac{ASV}{ASV + FBV}, \quad VE = \frac{FSV}{ASV + FBV}
\tag{7}
$$

based on the spot volume defined as: $V = \displaystyle\sum_{x,y \in \mathrm{Re}\,gion} I(x,y)$.

The spot volumes which are calculated according to Eq. (7) correspond to the "Actual Spot Volume" (*ASV*), "False Spot Volume" (*FSV*) and "False Background Volume" (*FBV*), respectively. Table 3 presents the results obtained by Melanie 7, Delta2D, PDQuest 8.0.1 and the presented segmentation scheme. It is evident that, the presented scheme outperforms all three software packages in terms of *VO* and *VE*. Moreover, the presented scheme demonstrates a remarkably lower variance in both performance measures, as a result of its robustness over streaks, multiplets and faint spots.
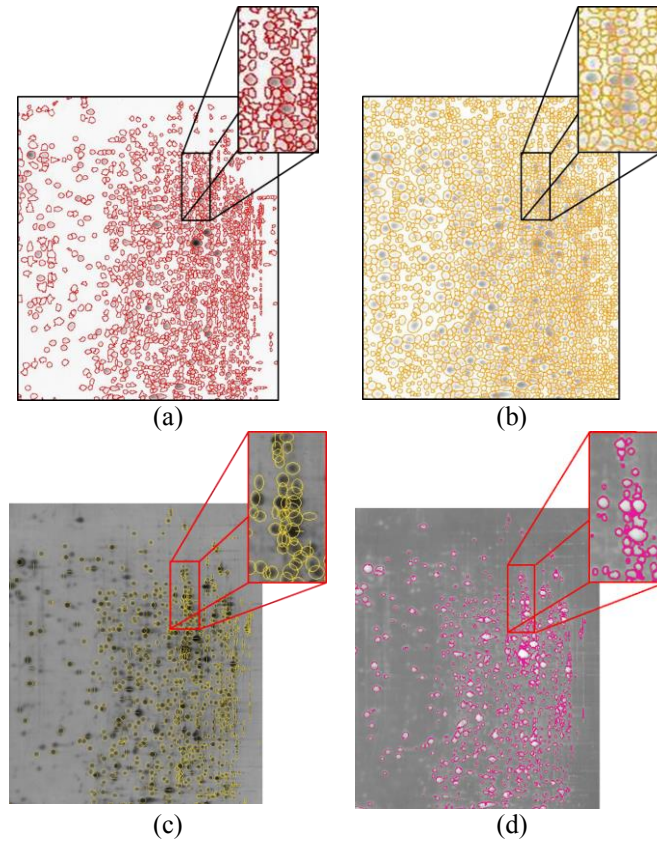

Fig. 6. Segmentation results obtained by the application of: (a) Melanie 7, (b) Delta2D, (c) PDQuest 8.0.1 and (d) the presented segmentation scheme.

Table 3: Segmentation results

	Melanie 7	Delta2D	PDQuest 8.0.1	Presented Scheme
VO	86.5±3.2%	82.4±3.6%	80.2±4.6%	92.0±1.2%
VE	55.0±6.7%	64.3±7.6%	83.1±8.9%	20.0±3.2%

4   Conclusions and Future Work

In this thesis, unsupervised image analysis algorithms have been presented for the detection and segmentation of various types of images focusing on proteomics and medical images. The presented framework for automated adjustment of region-based *AC* parameters was compared to the empirical fine-tuned version and achieved to: a) maintain a high segmentation quality comparable to the one stemmed from each empirically fine-tuned approach, b) speed up contour convergence by selectively amplifying data fidelity forces, c) enrich segmentation results with objectivity and reproducibility and d) relieve domain users from the tedious and time-consuming process of empirical adjustment. Additionally, the presented model for the detection and segmentation of proteomics images achieved to: a) endow detection and segmentation results with objectivity and reproducibility by automatically initializing the level set function based on regional intensity maxima associated with actual spots, b) generate more plausible spot boundaries than commercial image analysis software packages, c) outperform image analysis software packages in terms of *VO* and *VE* segmentation quality measures and d) provide an alternate to the laborious, error-prone and time-consuming process of manual editing, which is required by gel analysis experts in state-of-the-art *2D-GE* software packages.

Future work includes the investigation of active surfaces for 3D segmentation and machine learning algorithms for automated parameter adjustment.

References

[1]   T.F. Chan, L.A. Vese, Active contours without edges, IEEE Trans. Im. Proc. 10 (2) (2001) 266-277.

[2]   M.A. Savelonas, E.A. Mylona, D. Maroulis, Unsupervised 2D gel electrophoresis image segmentation based on active contours, Pattern Recognition 45 (2) (2012) 720-731.

[3]   E.A. Mylona, M.A. Savelonas, D. Maroulis, S. Kossida, A computer-based technique for automated spot detection in proteomics images, IEEE Trans. Inf. Tech. Biomed. 15 (4) (2011) 661-667.

[4]   E.A. Mylona, M.A. Savelonas, D. Maroulis, Automated adjustment of region-based active contour parameters using local image geometry, accepted with revisions to IEEE Trans. Cyber. (26/11/2013).

[5]   E.A. Mylona, M.A. Savelonas, D. Maroulis, Self-parameterized active contours based on regional edge structure for medical image segmentation," submitted to Med. & Biol. Eng. & Comp. (26/8/2013).

[6]   E.A. Mylona, M.A. Savelonas, D. Maroulis, Automated parameterization of active contours: a brief survey, in Proc. IEEE International Symposium on Signal Processing and Information Technology (ISSPIT), Athens, Greece, 2013.

[7]   E.A. Mylona, M.A. Savelonas, D. Maroulis, Self-adjusted active contours using multi-directional texture cues, in Proc. IEEE International Conference on Image Processing (ICIP), Melbourne, Australia, 2013.

[8]   E.A. Mylona, M.A. Savelonas, E. Zacharia, D. Maroulis, C. Pattichis, Unsupervised level set parameterization using multi-scale filtering, in Proc. IEEE International Conference on Digital Signal Processing (DSP), Santorini, Greece, 2013.

[9] E.A. Mylona, M.A. Savelonas, D. Maroulis, A.N. Skodras, Autopilot spatially-adaptive active contour parameterization for medical image segmentation, in Proc. IEEE International Symposium on Computer-Based Medical Systems (CBMS), Porto, Portugal, 2013.

[10] E.A. Mylona, M.A. Savelonas, D. Maroulis, Entropy-based spatially-varying adjustment of active contour parameters, in Proc. IEEE International Conference on Image Processing (ICIP), Orlando, FL, USA, 2012.

[11] M. Savelonas, E. Mylona, D. Maroulis, An automatically initialized level-set approach for the segmentation of proteomics images, in Proc. IEEE International Workshop on Biomedical Engineering, Kos, Greece, 2011.

[12] E.A. Mylona, M.A. Savelonas, D. Maroulis, M. Aivaliotis, 2D-GE image segmentation based on level-sets, in Proc. IEEE International Conference on Image Processing (ICIP), Brussels, Belgium, 2011.

[13] E. Mylona, M. Savelonas, D. Maroulis, A two-stage active contour-based scheme for spot detection in proteomics images, in Proc. IEEE International Conference on Information Technology Applications in Biomedicine (ITAB), Corfu, Greece, 2010.

[14] E. Mylona, M. Savelonas, D. Maroulis, Protein spot detection in 2D-GE images using morphological operators, in Proc. IEEE International Symposium on Computer-Based Medical Systems (CBMS), Perth, Australia, 2010.

[15] M. Savelonas, E. Mylona, D. Maroulis, A level set approach for proteomics image analysis, in Proc. European Signal Processing Conference (EUSIPCO), Aalborg, Denmark, 2010.

[16] M.A. Savelonas, D. Maroulis, E. Mylona, Segmentation of two-dimensional gel electrophoresis images containing overlapping spots, in Proc. IEEE International Conference on Information Technology Applications in Biomedicine (ITAB), Larnaca, Cyprus, 2009.

[17] E.A. Mylona, M.A. Savelonas, D. Maroulis, Towards self-parameterized active contours for medical image segmentation with emphasis on abdomen," A.S. El-Baz et al. (eds.), Abdomen and Thoracic Imaging: An Engineering & Clinical Perspective, Springer Science + Business Media, New York, 2014.

[18] E. Mylona, M. Savelonas, D. Maroulis, Computer-based methodology for protein spot detection and its contribution to health services, 14th Panhellenic Conference of the Greek Physicists Union, Kamena Vourla, Greece, 2012.

[19] M.N. Do, M. Vetterli, The Contourlet transform: an efficient directional multiresolution image representation, IEEE Trans. Im. Proc. 14 (12) (2005) 2091-2106.

[20] X. Bresson, S. Esedoglu, P. Vandergheynst, J. Thiran, S. Osher, Fast global minimization of the active contour/snake model, J. Math. Im. Vis. 28 (2) (2007) 151-167.

[21] C. Li, C. Xu, C. Gui, M.D. Fox, Distance regularized level set evolution and its application to image segmentation, IEEE Trans. Im. Proc. 19 (12) (2010) 3243-3254.

[22] W.R. Crum, O. Camara, D.L.G. Hill, Generalized overlap measures for evaluation and validation in medical image analysis, IEEE Trans. Med. Im. 25 (11) (2006) 1451-1461.

[23] D. Huttenlocher, G. Klanderman, W. Rucklidge, Comparing images using the Hausdorff distance, IEEE Trans. Patt. Anal. Mach. Intell. 15 (1993) 850-63.

[24] P. Soille. Morphological Image Analysis-Principles and Applications. Springer, Berlin, 1999.

[25] R.D. Appel, J.R. Vargas, P.M. Palagi, D. Walther, Melanie II – a third-generation software package for analysis of two-dimensional electrophoresis images: II. Algorithms, Electrophoresis 18 (1997) 2735-2748.

[26] S.M. Pizer, E.P Amburn, J.D. Austin, Adaptive histogram equalization and its variations, Comp. Vis. Graph. Im. Proc. 39 (1987) 355-368.

[27] J.I. Garrels, The QUEST system for quantitative analysis of two-dimensional gels, J. Biol. Chem. 264 (1989) 5269-5282.